phys. stat. sol. (a) 58, 115 (1980)

Subject classification: 14.4; 10.2; 22.6.1

Department of Inorganic Materials Science, Twente University of Technology, Enschede[1])

Electrical Conductivity of Fluorite and Pyrochlore $Ln_xZr_{1-x}O_{2-x/2}$ (Ln = Gd, Nd) Solid Solutions

By

T. VAN DIJK, K. J. DE VRIES, and A. J. BURGGRAAF

The ionic conductivity of ceramic $Gd_xZr_{1-x}O_{2-x/2}$ and $Nd_xZr_{1-x}O_{2-x/2}$ solid solutions is measured as a function of composition. Both solid solutions are of the defect fluorite type and the fluorite-related ordered pyrochlore phase is present around the stoichiometric compositions $Gd_2Zr_2O_7$ and $Nd_2Zr_2O_7$. As a function of composition the conductivity goes through a maximum for stoichiometric $Gd_2Zr_2O_7$ whereas the conductivity is minimal for $Nd_2Zr_2O_7$. It appears that at the stoichiometric pyrochlore composition both, activation enthalpy ΔH and pre-exponential factor σ_0 are minimal and that the absolute magnitude of the pre-exponential factor accounts for the difference in the net conductivity effect of the systems studied. The results obtained from both, single crystalline and ceramic samples can be correlated with the defect structure and ordering in the anion sublattice and with deviations of Vegard's law in the fluorite subcell dimensions. No discontinuity of σ_0 or ΔH is observed at the fluorite–pyrochlore phase boundary. This suggests the existence of a hybrid phase around the fluorite–pyrochlore phase boundary in this type of system.

Die Ionenleitfähigkeit von keramischen $Gd_xZr_{1-x}O_{2-x/2}$ und $Nd_xZr_{1-x}O_{2-x/2}$-Mischkristallen wird als Funktion der Zusammensetzung gemessen. Beide Mischkristalle sind vom Fluorit-Defekttyp und die fluoritverknüpfte geordnete Pyrochlorphase existiert um den Bereich der stöchiometrischen Zusammensetzungen $Gd_2Zr_2O_7$ und $Nd_2Zr_2O_7$. In Abhängigkeit von der Zusammensetzung durchläuft die Leitfähigkeit ein Maximum für stöchiometrisches $Gd_2Zr_2O_7$, während die Leitfähigkeit für $Nd_2Zr_2O_7$ minimal ist. Es zeigt sich, daß bei der stöchiometrischen Pyrochlorzusammensetzung sowohl die Aktivierungsenthalpie ΔH als auch der prä-exponentielle Faktor σ_0 minimal sind und daß die absolute Größe des prä-exponentiellen Faktors die Differenz in der Nettoleitfähigkeit der untersuchten Systeme erklärt. Die sowohl von einkristallinen als auch von keramischen Proben erhaltenen Ergebnisse lassen sich mit der Defektstruktur und der Ordnung im Anionenuntergitter und mit den Abweichungen der Abmessungen der Fluorit-Unterzellen von der Vegardschen Regel korrelieren. Es wird keine Diskontinuität von σ_0 oder ΔH an der Fluorit–Pyrochlor-Phasengrenze beobachtet. Dies weist auf die Existenz einer Hybridphase in der Nähe der Fluorit–Pyrochlor-Phasengrenze in diesem Systemtyp hin.

1. Introduction

Zirconia forms cubic solutions of the defect fluorite type with oxides of several divalent and trivalent metals. For substitution with Ln(III) oxide (where Ln is one of the lanthanide ions) the substitution reaction is

$$(1-x)\,ZrO_2 + \frac{x}{2}\,Ln_2O_3 \rightarrow Ln_xZr_{1-x}O_{2-x/2} + \frac{x}{2}\,V_O^{\cdot\cdot}\,. \qquad (1)$$

Hence this substitution gives rise to a defect concentration $x/4a_0^3$ in the anion sublattice where a_0 is the fluorite cell edge.

Depending both on the type of substituent ion as well as the temperature and oxygen pressure, interaction with atmosphere can take place according to either of the follow-

[1]) P.O. Box 217, 7500 AE Enschede, The Netherlands.

ing reactions:

$$V_O^{\cdot\cdot} + \tfrac{1}{2} O_2 \rightleftarrows O_O + 2h^{\cdot}, \quad (2)$$

$$O_O \rightleftarrows \tfrac{1}{2} O_2 + V_O^{\cdot\cdot} + 2e', \quad (3)$$

and hence under certain conditions p- or n-type electronic defects exist in these solids.

Due to the defects in the anion sublattice this type of compound exhibits fast oxygen diffusion, especially at elevated temperatures while the activation energy for oxygen diffusion is of the order of 100 kJ/mol.

As a function of substituent concentration these so-called stabilized zirconias usually exhibit a conductivity maximum at the low substitution side of the cubic phase field when the anion defect concentration is about 5%. Extensive reviews on this subject have been given by Etsell and Flengas [1] and more recently by Dell and Hooper [2]. Because of the high oxygen conductivity the stabilized zirconias can be applied as solid electrolytes in high-temperature fuel cells, oxygen monitoring and measuring systems and, because of their refractoriness, can also be used as MHD electrodes [3, 4].

As the anion vacancy concentration is increased it is supposed that conductivity decreases due to interactions of vacancies with each other and with cations, which effectively reduce the concentration of mobile vacancies. Moreover, substitution of larger ions for Zr^{4+} at the low substitution side of the cubic phase field may lead to a narrowing of the passages for the diffusing ions and hence causes an increase of the activation enthalpy for diffusion [5, 6]. However, the detailed nature of these phenomena is not well understood. Relaxation and ordering effects which may occur in the anion sublattice are strongly enhanced when there is also ordering in the cation sublattice [5].

In the case of calcia and yttria stabilized zirconia it was found that after prolonged annealing the conductivity can decrease considerably depending on annealing temperature and atmosphere. These ageing effects were studied by transmission electron microscopy and diffuse scattering was observed due to the intergrowth of small domains of $CaZr_4O_9$ [7] or of $CaZr_4O_9$ and monoclinic ZrO_2 [8] in calcia stabilized zirconia. However, neither the influence of cation ordering nor the ordering of anion vacancies in a number of possible vacancy superstructures, which are well known in defect fluorite-type $MO_{2-\delta}$ structures [9, 10] on ionic conductivity, are well understood.

For these reasons we investigated the conductivity in ZrO_2–Gd_2O_3 and ZrO_2–Nd_2O_3 solid solutions. In these systems the fluorite-type solid solutions exist in a wide composition range and, moreover, the compounds $Gd_2Zr_2O_7$ and $Nd_2Zr_2O_7$ exist with pyrochlore structure characterized by a long-range order of cation and anion vacancies.

The pyrochlore structure of stoichiometric $Ln_2Zr_2O_7$ (SG Fd3m) can be derived from the fluorite structure (SG Fm3m) by doubling the fluorite cell edge, placing the large Ln^{3+} ions at 16c, the smaller Zr^{4+} ions at 16d and the O^{2-} ions at 8a and 48f, leaving the fluorite position 8b vacant. The space group parameter x(48f) is about 0.41, due to the tendency of the remaining anions to shift in the direction of the vacant 8b positions. The structure can be described as a three-dimensional framework formed from vertex-sharing ZrO_6 octahedra. The seventh anion does not form part of this framework. The oxygen sublattice contains strings in the ⟨110⟩ directions where oxygen positions alternate between occupied and vacant.

It is possible to introduce a concentration of point defects (oxygen vacancies or interstitials) by substituting Ln^{3+} or Zr^{4+} ions, respectively, in the stoichiometric $Ln_2Zr_2O_7$. The extension and stability of the non-stoichiometric pyrochlore phases $Ln^{3+}_{2\pm x}Zr^{4+}_{2\mp x}O_{7\mp x}$ are mainly determined by the ionic radius ratio $r_{Ln^{3+}}/r_{Zr^{4+}}$ [11] and for this reason it is expected that the extension of the pyrochlore phase is larger for the

ZrO_2–Nd_2O_3 than for the ZrO_2–Gd_2O_3 system. A phase diagram for the ZrO_2–Gd_2O_3 system was given by Perez y Jorba [11] and for the ZrO_2–Nd_2O_3 system by Perez y Jorba [11] and Rouanet [12].

In the ZrO_2–Gd_2O_3 system the pyrochlore phase is bell-shaped within the defect fluorite phase. At 1000 °C the phase boundaries are at about 46 and 53 at% Gd^{3+}. The maximum pyrochlore–fluorite transition temperature is about 1550 °C at the stoichiometric composition $Gd_2Zr_2O_7$.

Disagreement exists in literature for the ZrO_2–Nd_2O_3 phase diagram. According to Perez y Jorba [11] the lower boundary of the cubic phase is at 22 mol% $NdO_{1.5}$, the pyrochlore single phase being located between 30 and 57 at% Nd^{3+}. According to Rouanet [12], however, the pyrochlore single phase is only found in a very narrow region around the stoichiometric $Nd_2Zr_2O_7$ composition, the hypo- and hyperstoichiometric compositions actually being two-phase mixtures of pyrochlore phase with cation disordered defect fluorite and Tl_2O_3 structure, respectively.

Our aim is to study the influence of both cation and anion vacancy ordering on the oxygen conductivity. Of special interest is the conductivity behaviour in the vicinity of the stoichiometric pyrochlore composition. If the oxygen vacancies are completely ordered in stoichiometric materials, vacancies are changed into non-occupied structural sites. The concentration of mobile species then varies strongly immediately around the stoichiometric composition while it is mainly determined by the intrinsic defect equilibria of the pyrochlore structure. Non-stoichiometric compositions can be considered as stoichiometric compounds doped with one of the end members of the binary system. This causes introduction of extrinsic defects in the oxygen sublattice. Both effects mentioned above will influence the conductivity and will be investigated.

2. Experimental Procedures

2.1 Preparation of specimens

Cubic solid solutions $Gd_xZr_{1-x}O_{2-x/2}$ and $Nd_xZr_{1-x}O_{2-x/2}$ with $0.2 < x < 0.6$ were prepared by means of a wet chemical method based upon the dropwise thermolysis of a viscous precursor consisting of a citrate complex of zirconia and lanthanide ions using ammonium nitrate as a swelling agent [13]. After 15 min calcination at 900 to 1000 °C the resulting powder consists of highly sinter-reactive "popcorn-like" powder agglomerates having crystallite sizes in the range of 100 to 150 Å and a purity of about 97.5%.

After granulating, powder compacts were isostatically pressed at 400 N/mm² reaching a green density of 48 to 51% of the theoretical density.

After preheating at 1300 °C for 48 h to remove remaining volatile impurities the pellets were sintered at 1550 °C for 70 h in an oxygen atmosphere. Cylindrical samples (discs) were then cut out of the pellets and subsequently annealed at 1000 °C for 100 h.

2.2 Characterization of specimens

After sintering at 1550 °C the density of the specimens, determined pycnometrically, is 92 to 97% of the theoretical density, based upon an oyxgen vacancy defect structure. As a result of the relatively low sintering temperature the average grain size of the specimens is then 2 to 4 μm as revealed by scanning electron microscopy on well-polished and thermally etched specimens. A well-developed ceramic microstructure with uniform grain size is present showing no visible impurities at the grain boundaries and with pores mainly situated at these boundaries (Fig. 1).

The composition of the samples was determined by X-ray fluorescence analysis,

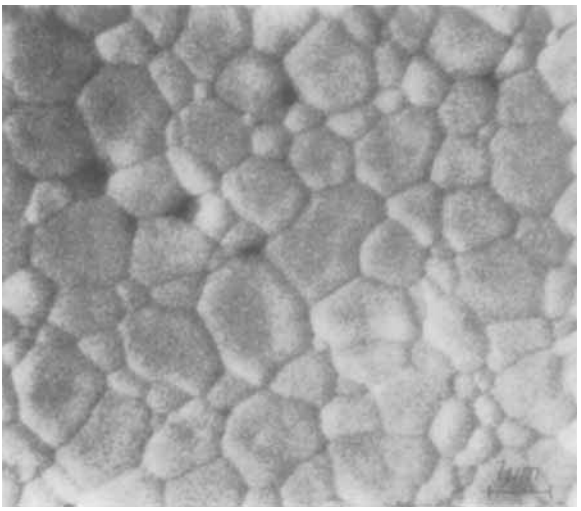

Fig. 1. Scanning electron micrograph of the microstructure of a ceramic $Gd_{0.50}Zr_{0.50}O_{1.75}$ sample, prepared via the citrate synthesis, sintered at 1550 °C during 70 h

having a relative accuracy better than 0.4%. This analysis also revealed that the final purity of the specimens is better than 99.5%. X-ray diffraction on ground material prepared in the manner just mentioned showed no second phase in either of the specimens. Comparison of the half-widths of the X-ray diffraction lines with those of a reference silicon standard revealed that the specimens were very homogeneous.

Specimens with compositions between 46 and 53 at% Gd^{3+} and specimens with compositions between 38 and 55 at% Nd^{3+} showed the characteristic pyrochlore superstructure reflections due to long-range ordering of cations. These results are for the ZrO_2–Gd_2O_3 system in accordance with the phase diagram given by Perez y Jorba [11].

Our X-ray and neutron powder refinement results of non-stoichiometric ZrO_2–Nd_2O_3 pyrochlore compositions support evidence for a hybrid crystal structure [14]. It should be pointed out that this is not a classical two-phase mixture according to the phase diagram proposed by Rouanet [12] as such a mixture assumes two phases with differing compositions and hence with differing lattice parameters which we did not observe.

2.3 Transference number determination

Ionic transference numbers were determined by means of the e.m.f. method using the oxygen partial pressures of air and pure oxygen. Therefore we constructed a concentration cell as depicted schematically in Fig. 2, which allowed us to handle samples in a quick and easy way without necessity of cooling the complete system down to room temperature when changing the samples. Samples with diameters of about 10 mm and thicknesses of 0.5 mm were used.

Care was taken to avoid temperature gradients larger than ± 0.5 K over the samples. This point was achieved by a heating system in the bottom gas flow and was checked by thermocouples near the sample (see 5 and 11 in Fig. 2). The outlets of both oxygen and air flows are provided with a liquid lock which allowed us to detect even small gas eakage along the samples by ceasing one of the flows. The samples were pressed down onto the well-polished top side of the silica tube (see 10 in Fig. 2) by a weight situated outside (see 1 in Fig. 2).

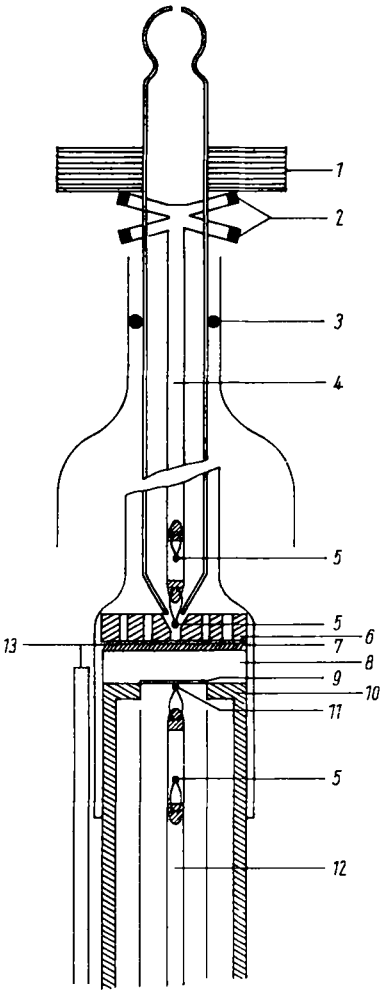

Fig. 2. Scheme of the concentration cell used for the e.m.f. measurements. 1 load; 2 thermocouple contacts; 3 o-ring seal; 4 gas flow (air) to the sample (8); 5 thermocouples; 6 alumina disc with holes used for centering and conveyance of the gas flow from the upper side to the sample; 7, 9 dc sputtered platinum electrodes; 8 sample, 10 top of silica tube; 11 combination of thermocouple and electrical contact; 12 gas flow (oxygen) to the sample (8), this gas flow is preheated to avoid temperature differences over the sample; 13 electrical contact

2.4 ac conductivity measurements

Porous platinum electrodes with thicknesses of about 2 μm were sputtered onto the ceramic sample discs and were then submitted to complex admittance measurements. For the frequency range 8×10^2 to 5×10^4 Hz a Wayne Kerr B 221 universal bridge was used with a sample voltage of 100 mV and for the frequency range 5×10^4 to 3×10^6 Hz a Wayne Kerr B 601 radio frequency bridge with a sample voltage of about 60 mV. Occasionally some samples were measured with a Solartron FRA 1172 apparatus in the frequency range 10^{-1} to 10^4 Hz enabling us to investigate the low frequency part of the complex admittance diagrams. All measurements were performed at temperatures between 500 and 750 °C in an air atmosphere.

Complex admittance measurements of samples plotted in complex plane diagrams [15] generally show a behaviour as shown in Fig. 3. The first semicircle can beattributed to electrode-interface polarization phenomena, the second one is caused by polarization phenomena at the grain boundaries [16]. The complex admittance diagrams can be represented phenomenologically by the equivalent circuit shown in Fig. 4. The high-frequency intercept with the σ'-axis yields the grain bulk conductivity.

We found that the shapes of bulk conductivity versus composition curves were not affected by grain size effects.

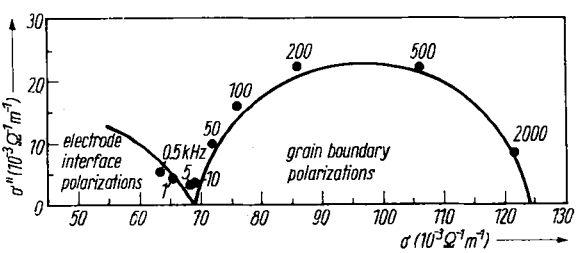

Fig. 3. Complex admittance diagram of $Gd_{0.51}Zr_{0.49}O_{1.745}$ at $T = 600$ °C

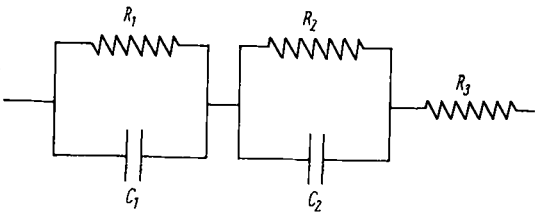

Fig. 4. Equivalent circuit representing the complex admittance behaviour of ceramic stabilized zirconia. R_1 and C_1 resistance and capacity of the electrode interface, R_2 and C_2 resistance and capacity of the grain boundaries, R_3 resistance of the grain bulk material

3. Results and Discussion

3.1 The lattice parameter as a function of compositions

The lattice parameters for the ZrO_2–Nd_2O_3 and ZrO_2–Gd_2O_3 systems as measured by us are combined with additional values given by other authors [11, 17 to 20] and are shown in Fig. 5 as a function of the composition parameter x at room temperature. For both systems the lattice parameter[2]) increases with increasing lanthanide ion content.

Perez y Jorba [11] has stated that for all lanthanide stabilized zirconias the cell parameter versus concentration curves show a bend at $x = 0.5$. We want to emphasize that there is another bend in these curves for $x = 0.35$ which was not noted before and is especially evident in the ZrO_2–Gd_2O_3 system.

The lattice parameter of fluorite and pyrochlore solid solutions $A_2Zr_2O_7$ increases linearly with increasing ionic radius of the A^{3+} ion as shown in Fig. 6, where we have plotted values measured and collected by Glushkova et al. [20]. It is obvious from Fig. 6 that the bend shown in Fig. 5 for $x = 0.35$ is not likely to be caused by the increase of the mean size of the cations or by long-range ordering of them. As the oxygen vacancy concentration also increases linearly with increasing lanthanide content, it is tempting to correlate this bend with the onset of the ordering of oxygen vacancies.

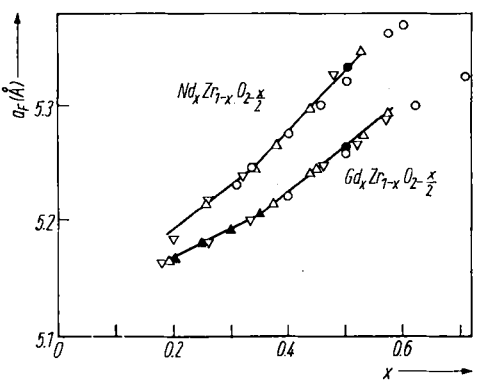

Fig. 5

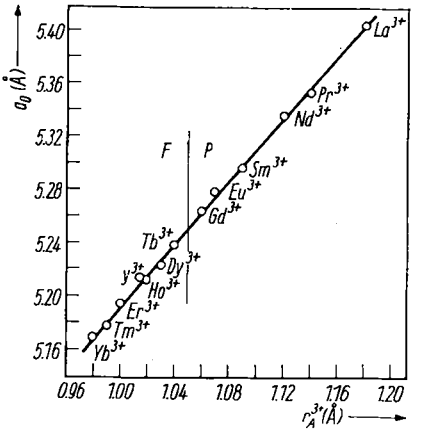

Fig. 6

Fig. 5. Lattice parameter as a function of composition in cubic solid solutions $Nd_xZr_{1-x}O_{2-x/2}$ and $Gd_xZr_{1-x}O_{2-x/2}$ with $0.2 < x < 0.6$. △ our results, ○ after [11], ▲ [17], ▽ [19], ● [20]

Fig. 6. Lattice parameter of fluorite and pyrochlore $A^{3+}_{0.50}Zr^{4+}_{0.50}O_{1.75}$ solid solutions as a function of effective ionic radius of A^{3+}. P pyrochlore phase, F fluorite phase

[2]) The parameter of the half pyrochlore cell and hence of the corresponding fluorite cell was taken for pyrochlore compositions.

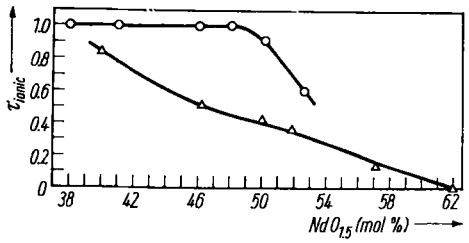

Fig. 7. Ionic transference number in the ZrO_2–$NdO_{1.5}$ system as a function of composition. ○ this work, △ after Volchenkova [21]

It will be shown in Section 3.3 that the compositions $x = 0.35$ and 0.5 mark special points in the conductivity behaviour of the ZrO_2–Gd_2O_3 system.

3.2 e.m.f. measurements

Results of e.m.f. measurements show that under the temperature and oxygen pressure conditions investigated (500 to 750 °C, $P^{I}_{O_2} = 0.2$ atm, $P^{II}_{O_2} = 1$ atm) the conductivity of the cubic ZrO_2–Gd_2O_3 solid solutions is almost purely ionic.

The results for $Nd_xZr_{2-x}O_{2-x/2}$ solid solutions show that up to $x = 0.5$ the conductivity is almost purely ionic, but for concentrations with $x > 0.5$ there is an appreciable electronic component. Our results in this system do not agree with those of Volchenkova [21] who found much larger electronic contributions in a wide composition range in this system, even for $x < 0.5$. Our results and those of Volchenkova [21] are visualized in Fig. 7.

3.3 Conductivity measurements

In Fig. 8 the grain bulk conductivities of samples in the ZrO_2–Gd_2O_3 system are plotted as a function of rare-earth content at 520, 620, and 720 °C. As a reference a sample containing 19.2 mol% $GdO_{1.5}$ was measured because around this value the conductivity is at its maximum [22]. The conductivities of the 19.2 mol% sample at the temperatures mentioned are 0.05, 0.27, and 0.93 $(\Omega\ m)^{-1}$, respectively, which are quite close to the values given in [22].

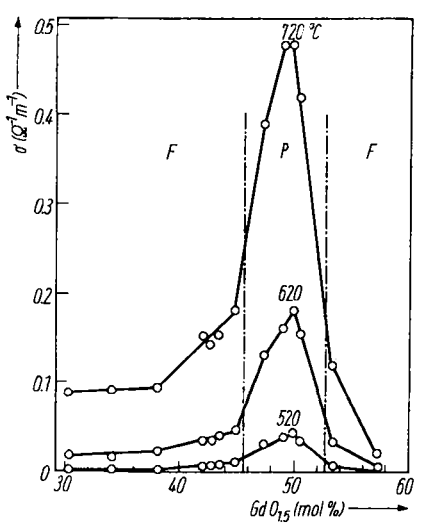

Fig. 8. Grain bulk conductivity at 520, 620, and 720 °C as a function of composition in the ZrO_2–$GdO_{1.5}$ system. F fluorite phase, P pyrochlore phase

From Fig. 8 it is now obvious that:

(i) the conductivity sharply decreases for compositions between about 19 and 30 mol% $GdO_{1.5}$;

(ii) from about 30 to about 38 mol% $GdO_{1.5}$ the conductivity remains practically constant;

(iii) starting at about 38 mol% $GdO_{1.5}$ the conductivity increases *continuously* until

it reaches a maximum at 50 mol% $GdO_{1.5}$ (composition $Gd_2Zr_2O_7$); in the pyrochlore phase the relative conductivity increase with composition appears to be larger than in the fluorite phase;

(iv) beyond the stoichiometric composition $Gd_2Zr_2O_7$ the conductivity strongly decreases;

(v) at low temperatures the conductivity of the pyrochlore phase is relatively large compared to the conductivity at the low substitution level in the fluorite phase.

The composition dependence of conductivity can be more easily understood if the results are analysed as a function of temperature. In the well-known Arrhenius-like equation,

$$\sigma = \frac{\sigma_0}{T} \exp\left(-\frac{\Delta H}{RT}\right), \tag{4}$$

σ_0 is a function of the effective number of mobile species and ΔH the activation enthalpy for migration [23].

It appears from Fig. 9, where the activation enthalpy is shown as a function of composition, that initially the activation enthalpy increases with increasing composition. This effect was previously observed in other zirconias stabilized with larger cations [5, 6] and was then qualitatively explained by the replacement of the small Zr^{4+} ions by the larger substituent ions. However, such an explanation does not account for either the *relative increase* of the lattice parameter with composition or for its effect on the activation enthalpy.

However, the most striking feature of Fig. 9 is the decrease of activation enthalpy for compositions between 35 and 60 mol% $GdO_{1.5}$ and the subsequent minimum at the stoichiometric pyrochlore composition $Gd_2Zr_2O_7$.

In Section 3.1 it was pointed out that in the lattice parameter versus concentration plot (Fig. 5) three distinct regions can be defined.

(i) $x < 0.35$: A relatively slow increase of the lattice parameter with composition. This results in a decrease of the mean size of a cation tetrahedron edge hence increasing the height of the potential barrier between adjacent occupied and vacant oxygen sites.

(ii) $0.35 < x < 0.50$: The lattice parameter increases relatively fast with increasing composition. The tetrahedron edges, especially those formed by two or three Zr^{4+} ions, are so enlarged that they lower the potential barrier between adjacent oxygen sites resulting in a decrease of the activation enthalpy.

(iii) $x > 0.50$: In this region two effects are involved, both resulting in an increase of the activation enthalpy. First there is the bend in the lattice parameter versus concentration curve already mentioned by Perez y Jorba [11] and second the tetra-

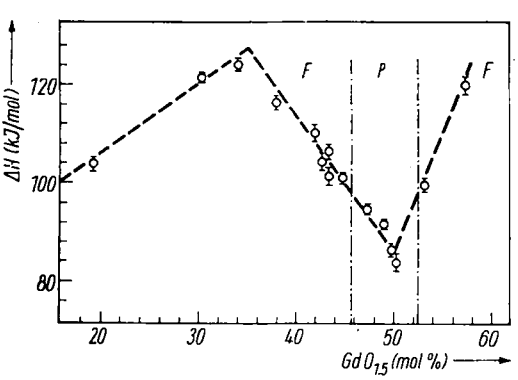

Fig. 9. Activation enthalpy for ionic conductivity as a function of composition in the ZrO_2-$GdO_{1.5}$ system

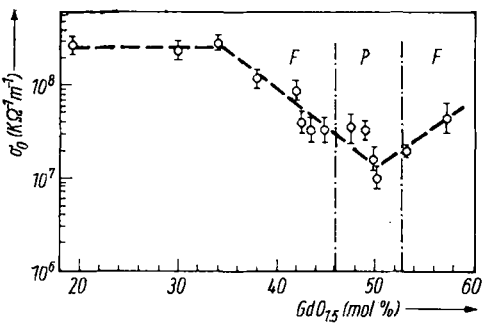

Fig. 10

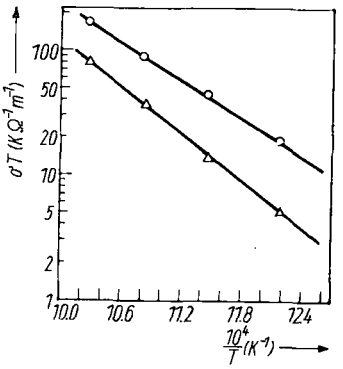

Fig.11

Fig. 10. Pre-exponential factor for ionic conductivity as a function of composition in the ZrO_2–$GdO_{1.5}$ system

Fig. 11. Grain bulk conductivity as a function of temperature for (○) an annealed (ordered) and (△) an as-grown (disordered) single crystal $Gd_{0.52}Zr_{0.48}O_{1.74}$. For the annealed sample: $\sigma_0 = 2.18 \times 10^7$ K $(\Omega\,m)^{-1}$, $\Delta H = 95.2$ kJ/mol; for the "as-grown" sample: $\sigma_0 = 1.64 \times 10^8$ K $(\Omega\,m)^{-1}$, $\Delta H = 117.5$ kJ/mol

hedron edges are now formed by at least two large Gd^{3+} ions so that the potential barrier between adjacent oxygen sites is again increased.

It can be seen from Fig. 10, where σ_0 versus $GdO_{1.5}$ content is shown, that the pre-exponential factor is practically constant up to about 35 mol% $GdO_{1.5}$ and then starts to decrease to a minimum value at the stoichiometric composition $Gd_2Zr_2O_7$. Roughly the pre-exponential factor appears to be a factor of about 20 smaller at the stoichiometric composition than at compositions having less than 35 mol% $GdO_{1.5}$.

The influence of long-range order on the activation enthalpy and the pre-exponential factor is also demonstrated by Fig. 11. Here the conductivity is plotted both for a single crystal $Gd_{0.52}Zr_{0.48}O_{1.76}$ annealed at 1250 °C during 20 h showing pyrochlore X-ray reflections and for an "as-grown" and quenched single crystal of the same composition which did not show these superstructure reflections. The annealed sample has an activation enthalpy and pre-exponential factor comparable with values graphically shown in Fig. 9 and 10, obtained from polycrystalline samples. The values of the "as-grown" sample are higher, again indicating a higher activation enthalpy and pre-exponential factor in the disordered structure when compared with the ordered structure.

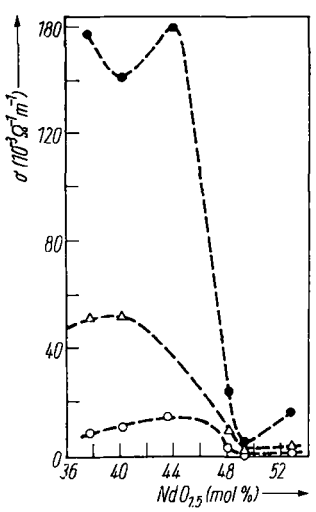

Fig. 12. Grain bulk conductivity as a function of composition in the pyrochlore phase of the ZrO_2–Nd_2O_3 system at various temperatures. ● 700, △ 600, ○ 500 °C

The compositional behaviour of conductivity for $Nd_xZr_{1-x}O_{2-x/2}$ solid solutions is shown in Fig. 12. It can be seen that for this system a deep conductivity *minimum* occurs at the stoichiometric composition $Nd_2Zr_2O_7$. The behaviour of ΔH and σ_0 versus composition is, however, similar for both systems. Both activation enthalpy (ΔH) and pre-exponential factor (σ_0) have a minimum value at the stoichiometric pyrochlore composition $Nd_2Zr_2O_7$ (Fig. 13, 14).

The decrease of activation enthalpy with composition for the $Nd_xZr_{1-x}O_{2-x/2}$ solid solutions studied with $x < 0.5$ is again predicted by the relatively large increase of the lattice parameter with the composition in this composition range.

The difference in conductivity behaviour of the ZrO_2–Gd_2O_3 and ZrO_2–Nd_2O_3 systems is mainly due to the anomalously low value of the pre-exponential factor for $Nd_2Zr_2O_7$. This anomaly is caused by the different defect structures of both systems.

Our neutron refinement results [16] show that stoichiometric $Nd_2Zr_2O_7$ has an almost perfect pyrochlore structure but that hypo- and hyperstoichiometric $Nd_xZr_{1-x}O_{2-x/2}$ pyrochlore compositions are partially disordered in the anion sublattice as is revealed by the occupation of the 8b position which is zero only for an ideally stoichiometric pyrochlore.

The concentration of intrinsic defects at a given temperature is larger for $Gd_2Zr_2O_7$ than for $Nd_2Zr_2O_7$. This can be made plausible from the lower stability of $Gd_2Zr_2O_7$ with respect to $Nd_2Zr_2O_7$, which is reflected by differences in melting point and disordering temperature.

Comparison of Fig. 10 and 14 shows that the pre-exponential factor for hypostoichiometric $Nd_xZr_{1-x}O_{2-x/2}$ pyrochlore is somewhat smaller, but well comparable with fluorite $Gd_xZr_{1-x}O_{2-x/2}$ with $x < 0.44$. Indeed for a nonstoichiometric pyrochlore with a relatively large excess of oxygen ions with respect to the oxygen concentration in stoichiometric pyrochlore, the influence of intrinsic defects as present in stoichiometric pyrochlore is negligible.

It can be easily seen from Fig. 8 to 10 that no discontinuity exists in the curves for σ, E, and σ_0 at the fluorite–pyrochlore phase boundary of the ZrO_2–Gd_2O_3 system. However, the σ_0 and lattice parameter versus composition curves show a bend and in

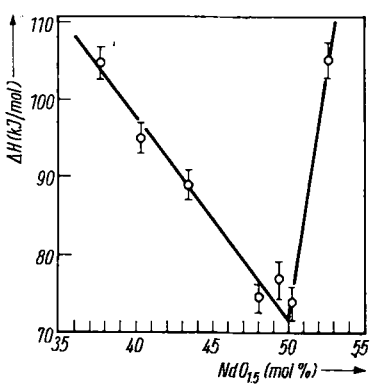

Fig. 13

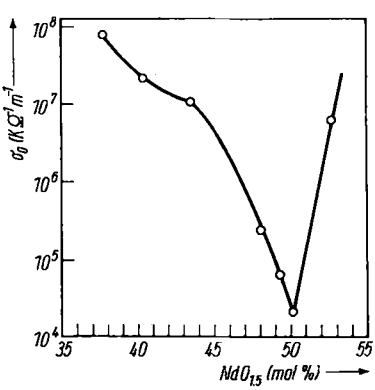

Fig. 14

Fig. 13. Activation enthalpy for ionic conductivity as a function of concentration in the pyrochlore phase of the ZrO_2–$NdO_{1.5}$ system

Fig. 14. Pre-exponential factor for ionic conductivity as a function of concentration in the pyrochlore phase of the ZrO_2–$NdO_{1.5}$ system

particular the activation enthalpy has a maximum at $x = 0.35$. The same holds essentially for the ZrO_2–Nd_2O_3 system. This follows when our results (Fig. 12 to 14) are compared with literature data on the low substitution side of this system [21, 22].

If the maximum at $x = 0.35$ is due to ordering phenomena in the anion sublattice, possibly accompanied by short-range order in the cation sublattice, the continuity at the fluorite–pyrochlore phase boundary strongly supports the occurrence of a hybrid phase in this type of system. The fluorite–pyrochlore phase boundary then separates a region of small pyrochlore-like regions in a defect fluorite matrix and of fluorite-like regions in a pyrochlore matrix.

The hybrid phase is then an intermingled structure of ordered and disordered regions, separated by continuous coherent boundaries. If such a hybrid system consists of both a well and a poor conducting phase, the overall conductivity of the system has to be described by a percolation process as both types of regions coexist in more or less comparable concentrations.

Acknowledgements

The authors would like to thank Dr. M. Perez y Jorba, CNRS, Vitry, France, for providing the single crystals mentioned in this paper and Ir. H. H. I. den Ouden for carrying out part of the conductivity measurements.

References

[1] T. H. Etsell and S. N. Flengas, Chem. Rev. **70**, 339 (1970).
[2] R. M. Dell and A. Hooper, in: Solid Electrolytes, Ed. P. Hagenmuller and W. van Gool, Academic Press, New York 1979 (p. 291).
[3] H. P. R. Frederikse and W. R. Hosler, Proc. XV. Symp. Engineering Aspects of MHD, Philadelphia 1976 (p. IV. 4.22).
[4] J. P. Coutures, G. Benezech, and F. Sibrende, High Temperatures – High Pressures **8**, 515 (1976).
[5] R. E. Carter and W. L. Roth, in: Electromotive Force Measurements in High-Temperature Systems, Ed. C. B. Alcock, The Institution of Chemistry and Metallurgy, London 1967 (p. 125).
[6] A. I. Ioffe, D. S. Rutman, and S. V. Karpachov, Electrochim. Acta **23**, 141 (1978).
[7] J. G. Allpress and H. J. Rossell, J. Solid State Chem. **15**, 68 (1975).
[8] B. Hudson and P. T. Moseley, J. Solid State Chem. **19**, 383 (1976).
[9] R. L. Martin, J. Chem. Soc. Dalton 1335 (1974).
[10] T. C. Parks and W. W. Barker, J. Solid State Chem. **20**, 397 (1977).
[11] M. Perez y Jorba, Thesis, Paris 1962.
[12] A. Rouanet, Rev. internat. houtes Temp. et Réfract. **8**, 161 (1971).
[13] M. A. C. G. van de Graaf, T. van Dijk, M. A. de Jongh, and A. J. Burggraaf, Science of Ceramics, Vol. 9, Ed. K. J. de Vries, De Nederlandse Keramische Vereniging, Enschede 1977 (p. 75).
[14] T. van Dijk, R. B. Helmholdt, and A. J. Burggraaf, to be published.
[15] J. E. Bauerle, J. Phys. Chem. Solids **30**, 2657 (1969).
[16] T. van Dijk, and A. J. Burggraaf, to be published.
[17] R. Collongues, M. Perez y Jorba, and J. Lefèvre, C. R. Acad. Sci. (France) **249**, 2329 (1959).
[18] J. Lefèvre, M. Perez y Jorba, and R. Collongues, Bull. Soc. Chim. (France) 1969 (1959).
[19] V. I. Strakhov, Ya. V. Klyucharov, and G. G. Sergeev, Zh. prikl. Khim. **46**, 2083 (1973).
[20] V. B. Glushkova, F. Hanic, and L. V. Sazonova, Ceramurgia internat. **4**, 176 (1979).
[21] Z. S. Volchenkova, Izv. Akad. Nauk SSR, Ser. neorg. Mater. **5**, 1096 (1969).
[22] H. Tannenberger, H. Schachner, and P. Kovacs, Rev. Energie primaire **2**, 19 (1966).
[23] A. S. Nowick and D. S. Park, in: Superionic Conductors, Ed. G. D. Mahan and W. L. Roth, Plenum Press, London 1976 (p. 395).

(Received November 13, 1979)